
Overview of $\bar{K}N$ and \bar{K} -nucleus dynamics

Avraham Gal

Received: date / Accepted: date

Abstract The main features of coupled-channel $\bar{K}N$ dynamics near threshold and its repercussions in few-body \bar{K} -nuclear systems are briefly reviewed highlighting the $I = 1/2$ $\bar{K}NN$ system. For heavier nuclei, the extension of mean-field calculations to multi- \bar{K} nuclear quasibound states is discussed focusing on kaon condensation.

Keywords $\bar{K}N$ dynamics · \bar{K} -nuclear quasibound states

PACS 13.75.Jz · 21.45.-v · 21.65.Jk · 21.85.+d · 36.10.Gv

1 Introduction

The \bar{K} -nucleus interaction near threshold is strongly attractive and absorptive as suggested by fits to the strong-interaction shifts and widths of K^- -atom levels [1,2]. Global fits yield extremely deep density dependent optical potentials with nuclear-matter depth $\text{Re}V_{\bar{K}}(\rho_0) \sim -(150-200)$ MeV at threshold. Chirally based coupled-channel models that fit the low-energy K^-p reaction data, and the $\pi\Sigma$ spectral shape of the $\Lambda(1405)$ resonance, yield moderate depths $\text{Re}V_{\bar{K}}(\rho_0) \sim -100$ MeV, as summarized recently in Ref. [3]. A major uncertainty in these chirally based studies arises from fitting the $\Lambda(1405)$ resonance by the imaginary part of the $\pi\Sigma(I=0)$ amplitude calculated within the same coupled channels chiral scheme. A third class, of shallower potentials with $\text{Re}V_{\bar{K}}(\rho_0) \sim -(40-60)$ MeV, was obtained by imposing a Watson-like self-consistency requirement [4]. However, one needs then to worry about higher orders in the chiral expansion which are not yet in.

I start by making introductory remarks on the $\bar{K}N - \pi\Sigma$ system, followed by reviewing two topics related to \bar{K} nuclear quasibound states: (i) the K^-pp system as a prototype of few-nucleon quasibound states of \bar{K} mesons; and (ii) multi- \bar{K} nucleus quasibound states. In reviewing the latter topic I will discuss the phenomenological evidence for the ‘extremely deep’ \bar{K} -nucleus potentials used in nuclear and nuclear-matter calculations.

Avraham Gal
Racah Institute of Physics, The Hebrew University, Jerusalem 91904, Israel
E-mail: avragal@vms.huji.ac.il

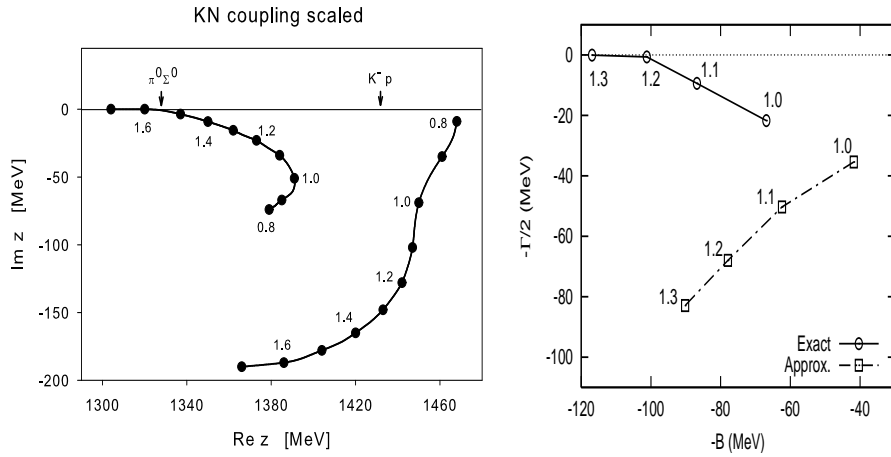


Fig. 1 Left: trajectories of Gamow poles in the complex energy (z) plane, on the Riemann sheet $[\Im k_{\bar{K}N}, \Im k_{\pi\Sigma}] = [+,-]$, upon scaling the $\bar{K}N$ interaction strengths (taken from Ref. [5]). The $\pi^0 \Sigma^0$ and $K^- p$ thresholds are marked by arrows. Right: $\bar{K}NN(I=1/2)$ quasibound state energy from Ref. [6] as a function of the $\bar{K}N$ interaction strength within a three-body coupled channel calculation (circles) and within a single channel approximate calculation (squares).

2 Polology of $\bar{K}N - \pi\Sigma$ coupled channels

Modern chirally motivated $\bar{K}N - \pi\Sigma$ coupled-channel models give rise to *two* Gamow poles that dominate low-energy $\bar{K}N$ dynamics. Representative pole positions are shown on the left-hand side of Fig. 1 for the coupled channels model of Ref. [7], together with the trajectories followed by these poles upon scaling the $\bar{K}N$ interactions. This model fits well all the low-energy $K^- p$ scattering and reaction data. It reproduces reasonably well the $\pi\Sigma$ spectrum shape, identified with the $\Lambda(1405)$ $\pi\Sigma$ resonance, which is determined primarily by the lower pole at (1391, $-i51$) MeV. This identification is further supported by the trajectory of the lower pole which merges into an $I=0$ genuinely bound state below the $\pi^0 \Sigma^0$ threshold when the $\bar{K}N$ interactions are sufficiently increased. The upper pole, in this model, is located above the $K^- p$ threshold. However, its position and the trajectory it follows away from the real energy axis are model dependent and sensitive to off-shell effects.¹ As discussed below in Sect. 3, the upper pole affects significantly the three-body $[\bar{K}(NN)_{I=1} - \pi\Sigma N]_{I=1/2}$ dynamics of the $K^- pp$ system. The energy and width of the ($\bar{K}NN$ quasibound - $\pi\Sigma N$ resonance) state are determined by a Gamow pole whose trajectory, from Ref. [6], is depicted in circles on the right-hand side of Fig. 1. Similarly to the lower-pole $\Lambda(1405)$ trajectory in the two-body case, this three-body pole also merges below the $\pi\Sigma N$ threshold into a genuinely bound state which, upon extending the model space, becomes a quasibound $\pi\Sigma N$ state decaying to lower channels ignored here.²

¹ For example, the pole positions in Ref. [8] are $z_> = 1428 - i17$, $z_< = 1400 - i76$ MeV.

² The other trajectory, depicted in squares, is relevant only to the discussion in Sect. 3.

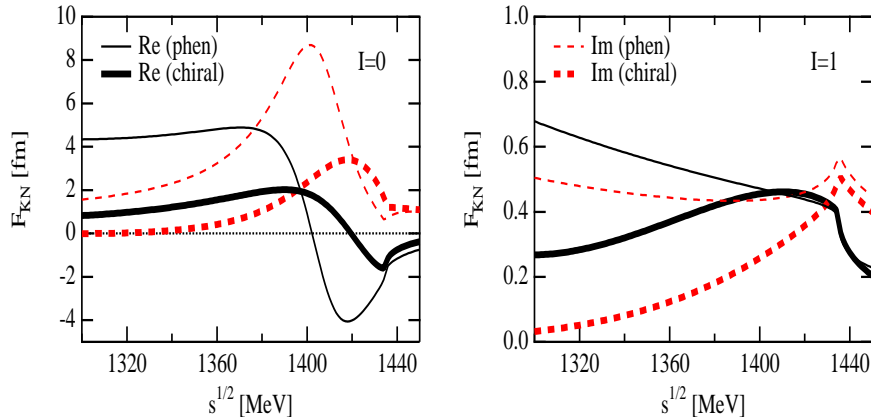


Fig. 2 Comparison of the Yamazaki-Akaishi phenomenological $\bar{K}N$ amplitudes [14] with the Hyodo-Weise chirally based $\bar{K}N$ amplitudes [8]. Figure taken from Ref. [8].

Table 1 Calculated B_{K^-pp} , mesonic (Γ_m) & nonmesonic (Γ_{nm}) widths (in MeV) of K^-pp .

	$\bar{K}NN$ single channel		$\bar{K}NN - \pi\Sigma N$ coupled channels		
	ATMS [13,14]	AMD [15]	Faddeev [16]	Faddeev [17]	variational [18]
B_{K^-pp}	48	17–23	50–70	60–95	40–80
Γ_m	61	40–70	90–110	45–80	40–85
Γ_{nm}	12	4–12			~ 20

3 Few-nucleon \bar{K} systems

The lightest \bar{K} nuclear configuration maximizing the strongly attractive $I = 0$ $\bar{K}N$ interaction is $[\bar{K}(NN)_{I=1}]_{I=1/2, J^\pi=0^-}$, loosely denoted as K^-pp . The FINUDA collaboration presented evidence in K^- stopped reactions on several nuclear targets for the process $K^-pp \rightarrow \Lambda p$, interpreting the observed signal as due to a K^-pp deeply bound state with $(B, \Gamma) \approx (115, 67)$ MeV [9]. However, this interpretation has been challenged in Refs. [10,11]. A preliminary new analysis of DISTO $pp \rightarrow K^+\Lambda p$ data was presented in EXA08 suggesting a K^-pp signal with $(B, \Gamma) \approx (105, 118)$ MeV [12]. The location practically on top of the $\pi\Sigma N$ threshold, and particularly the large width, are at odds with any of the few-body calculations listed below, posing a problem for a K^-pp quasibound state interpretation.

Results of few-body calculations for the K^-pp system are displayed in Table 1. The marked difference between the ‘ $\bar{K}NN$ single channel’ binding energies B_{K^-pp} reflects the difference between the input $\bar{K}N$ amplitudes shown in Fig. 2: the Yamazaki-Akaishi $I = 0$ single-pole amplitude [13] resonates at 1405 MeV, whereas the Dote-Hyodo-Weise $I = 0$ amplitude [15] resonates at 1420 MeV (close to the upper of two poles). This dependence on the input amplitudes has been verified in coupled-channel Faddeev calculations [6,19] and in variational calculations [18].

A notable feature of the K^-pp coupled-channel calculations [16,17,18] in Table 1 is that the explicit use of the $\pi\Sigma N$ channel adds about 20 ± 5 MeV to the binding energy calculated using effective $\bar{K}N$ potential within a single-channel calculation. This is

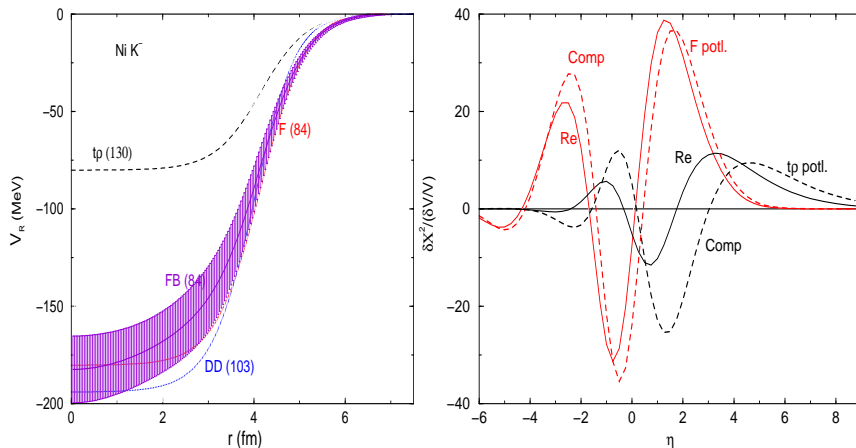


Fig. 3 Comparisons between density dependent potentials (DD, FB, F) and a $t\rho$ potential fitted to kaonic-atom data [2]. Left: the real part of the $\bar{K} - {}^{58}\text{Ni}$ potential. Right: functional derivatives of kaonic atoms χ^2 with respect to the fully complex (Comp, dashed) and real (Re, solid) potential as a function of $\eta = (r - R_c)/a_c$ using 2pF charge density distributions.

demonstrated on the right-hand side of Fig. 1 by comparing corresponding points on the two trajectories shown there.

4 \bar{K} -nucleus potentials from kaonic atoms and from nuclear reactions

Figure 3 (left) illustrates the real part of the best-fit \bar{K} -nucleus potential for ${}^{58}\text{Ni}$ as obtained for several models. The corresponding values of χ^2 for 65 K^- -atom data points are given in parentheses. A Fourier-Bessel (FB) fit [20] is also shown, within an error band. Just three terms in the FB series, added to a $t\rho$ potential, suffice to achieve a χ^2 as low as 84 and to make the potential extremely deep, in agreement with the density-dependent best-fit potentials DD and F. In particular, the density dependence of potential F provides by far the best fit ever reported for any global K^- -atom data fit, and the lowest χ^2 value as reached by the model-independent FB method.

The functional derivative (FD) method for identifying the radial regions to which exotic atom data are sensitive is demonstrated in Fig. 3 (right) for the F and $t\rho$ best-fit potentials [20]. It is clear that whereas within the $t\rho$ potential there is no sensitivity to the interior of the nucleus, the opposite holds for the density dependent F potential which accesses regions of full nuclear density. This owes partly to the smaller imaginary part of F, which also explains why the FD for the complex F potential is well approximated by that for its real part.

A fairly new and independent evidence in favor of extremely deep \bar{K} -nucleus potentials is provided by (K^-, n) and (K^-, p) spectra taken at KEK on ${}^{12}\text{C}$ [21] and very recently also on ${}^{16}\text{O}$ (presented in PANIC08) at $p_{K^-} = 1 \text{ GeV}/c$. The ${}^{12}\text{C}$ spectra are shown in Fig. 4, where the solid lines on the left-hand side represent calculations (outlined in Ref. [22]) using potential depths in the range 160-190 MeV. The dashed lines correspond to using relatively shallow potentials of depth about 60 MeV which I consider therefore excluded by these data.

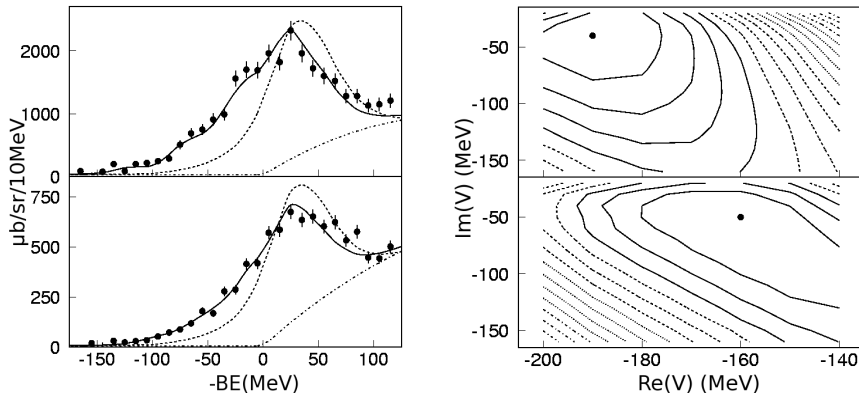


Fig. 4 KEK-PS E548 missing mass spectra (left) and χ^2 contour plots (right) for (K^-, n) (upper) & (K^-, p) (lower) at $p_{K^-} = 1$ GeV/c on ^{12}C [21].

In conclusion, optical potentials derived from the observed strong-interaction effects in kaonic atoms and from (K^-, N) nuclear spectra are sufficiently deep to support strongly-bound antikaon states. However, a fairly sizable extrapolation is required to argue for \bar{K} -nuclear quasibound states at energies of order 100 MeV below threshold, using a potential determined largely near threshold.

5 Multi- \bar{K} nucleus quasibound states from RMF calculations

Relativistic mean field (RMF) calculations of single- and of multi- \bar{K} nuclei are reported in these Proceedings by J. Mareš. Dynamical calculations of single- \bar{K} medium and heavy nuclei produce quasibound states bound by 100-150 MeV for potentials compatible with K^- atom data. These calculations also provide a quantitative estimate of the expected widths, which are larger than 100 MeV near threshold and remain of order 50 MeV or more, even as the primary $\bar{K}N \rightarrow \pi\Sigma$ decay mode shuts off at about 100 MeV below threshold [10, 23]. Highlights of multi- \bar{K} nuclear calculations are demonstrated here in Fig 5. On the left-hand side, results of RMF calculations are shown for $2n + \kappa\bar{K}^0$ systems, where all decay channels are suppressed. For $\kappa = 1$, the \bar{K}^0nn system which is charge symmetric to K^-pp was found to be unbound, apparently because RMF calculations do not allow for a $\bar{K}N - \pi\Sigma$ channel coupling. Binding within these schematic calculations starts at $\kappa = 2$ if isovector degrees of freedom are treated properly (say, using SU(3)) and for $\kappa = 3$ if they are suppressed. The \bar{K}^0 separation energy, denoted $B_{\bar{K}}$, is found to decrease with κ which is a special case of the saturation property established in heavier system, as discussed below.

K^- separation energies B_{K^-} in multi- K^- nuclei $^{40}\text{Ca} + \kappa K^-$ are shown on the right-hand side of Fig. 5 for two choices of $g_{\sigma K}$, designed within each RMF model to produce $B_{K^-} = 100$ and 130 MeV for $\kappa = 1$. A robust saturation of B_{K^-} with κ , independently of the applied RMF model, emerges from these calculations. The saturation values of B_{K^-} do not allow conversion of Λ hyperons to \bar{K} mesons through strong decays $\Lambda \rightarrow p + K^-$ or $\Xi^- \rightarrow \Lambda + K^-$ in multi-strange hypernuclei, which there-

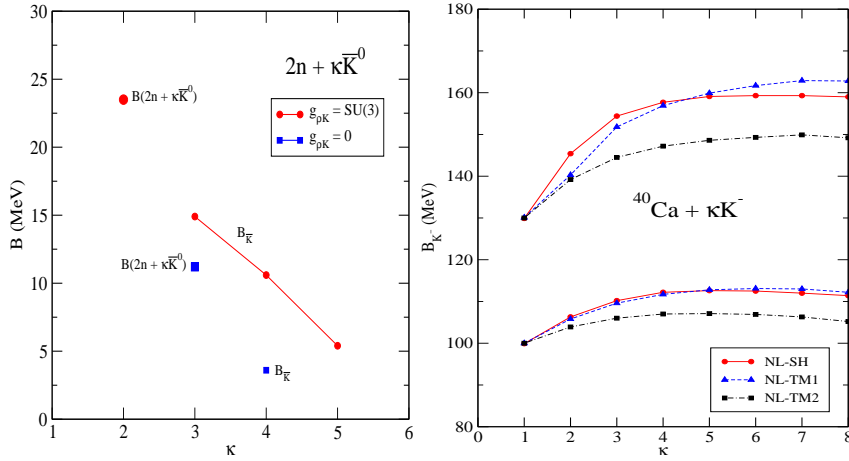


Fig. 5 RMF calculations of multi- \bar{K} nucleus quasibound states as function of the number κ of \bar{K} mesons. Left: for two neutrons, demonstrating the isovector effect. Right: for ^{40}Ca core, for several nuclear RMF models, with two choices of parameters fixed for $\kappa = 1$ [24].

fore remain the lowest-energy configuration for multi-strange systems. This provides a powerful argument against \bar{K} condensation in the laboratory, under strong-interaction equilibrium conditions [24, 25]. It does not apply to kaon condensation in neutron stars, where equilibrium configurations are determined by weak-interaction conditions.

Acknowledgements I am indebted to my collaborators Aleš Cieplý, Eli Friedman, Daniel Gazda and Jiří Mareš for instructive discussions and fruitful cooperation. This research was supported in part by the Israel Science Foundation, Jerusalem, grant 757/05.

References

1. C.J. Batty, E. Friedman, A. Gal, Phys. Rep. **287**, 385 (1997).
2. E. Friedman, A. Gal, Phys. Rep. **452**, 89 (2007).
3. W. Weise, R. Härtle, Nucl. Phys. A **804**, 173 (2008).
4. A. Ramos, E. Oset, Nucl. Phys. A **671**, 481 (2000).
5. A. Cieplý, A. Gal, arXiv:0809.0422 [nucl-th].
6. Y. Ikeda, T. Sato, Phys. Rev. C **79**, 035201 (2009).
7. A. Cieplý, J. Smejkal, Eur. Phys. J. A **34**, 237 (2007).
8. T. Hyodo, W. Weise, Phys. Rev. C **77**, 035204 (2008); and these Proceedings.
9. M. Agnello *et al.*, Phys. Rev. Lett. **94**, 212303 (2005).
10. J. Mareš, E. Friedman, A. Gal, Nucl. Phys. A **770**, 84 (2006).
11. V.K. Magas, E. Oset, A. Ramos, H. Toki, Phys. Rev. C **74**, 025206 (2006).
12. T. Yamazaki *et al.*, these Proceedings, arXiv:0810.5182 [nucl-ex].
13. T. Yamazaki, Y. Akaishi, Phys. Lett. B **535**, 70 (2002).
14. Y. Akaishi, T. Yamazaki, Phys. Rev. C **65**, 044005 (2002) [Eq. (29)].
15. A. Doté, T. Hyodo, W. Weise, Nucl. Phys. A **804**, 197 (2008); Phys. Rev. C **79**, 014003 (2009).
16. N.V. Shevchenko, A. Gal, J. Mareš, Phys. Rev. Lett. **98**, 082301 (2007).
17. Y. Ikeda, T. Sato, Phys. Rev. C **76**, 035203 (2007).
18. S. Wycech, A.M. Green, Phys. Rev. C **79**, 014001 (2009).
19. N.V. Shevchenko, A. Gal, J. Mareš, J. Révai, Phys. Rev. C **76**, 044004 (2007).
20. N. Barnea, E. Friedman, Phys. Rev. C **75**, 022202(R) (2007).
21. T. Kishimoto *et al.*, Prog. Theor. Phys. **118**, 181 (2007); Nucl. Phys. A **827**, 321c (2009).

-
22. J. Yamagata, H. Nagahiro, S. Hirenzaki, Phys. Rev. C **74**, 014604 (2006).
 23. D. Gazda, E. Friedman, A. Gal, J. Mareš, Phys. Rev. C **76**, 055204 (2007).
 24. D. Gazda, E. Friedman, A. Gal, J. Mareš, Phys. Rev. C **77**, 045206 (2008).
 25. D. Gazda, E. Friedman, A. Gal, J. Mareš, Phys. Rev. C **80**, 035205 (2009).